

# Development and Performance Evaluation of Graphene-Enhanced Polycrystalline Diamond Compact Cutter

Pei JU\*, Chuanliu WANG\*

**Abstract:** In order to improve the wear resistance, impact toughness and other comprehensive properties of PDC cutter, a new type of graphene-enhanced PDC cutter was developed by taking advantage of the excellent mechanical and thermal properties of graphene. Through the research of raw material treatment, diamond micro powder ratio, cemented carbide substrate structure and synthetic sintering process, three kinds of PDC cutters with graphene mass percentage of 0,1 wt%, 0,2 wt% and 0,3 wt% were prepared respectively. SEM tests showed that the binder distribution of PDC cutters with graphene mass percentage of 0,1 wt% and 0,2 wt% is relatively uniform, and there are no graphene agglomeration phenomenon occurred. Heat resistance tests showed that the heat resistance of the PDC cutter with graphene mass percentage of 0,2 wt% is the highest. Abrasion resistance tests showed that the wear ratio of the PDC cutter with graphene mass percentage of 0,2 wt% is the highest. Impact resistance tests showed that the impact energy of the PDC cutters with graphene mass percentage of 0,2 wt% and 0,3 wt% is the highest, and the impact resistance energy is over 2500 J. The Multiple Attribute Decision Making method was used to select the best graphene added scheme, and the PDC cutter with graphene mass percentage of 0,2 wt% shows the best comprehensive performance. The real drilling test was carried out in the Baiping Coal Mine of Zhengmei Group, the concave drill bit with 0,2 wt% graphene added PDC cutters showed the fastest average ROP, the least cutter wear, and the best drilling effect.

**Keywords:** graphene; PDC cutter; performance test; preparation technology

## 1 INTRODUCTION

With the increasingly complex geological conditions of coalbed methane gas extraction (drainage) drilling construction, the formations with high hardness, strong abrasive and severe heterogeneity were often encountered. As a pioneer of rock breaking, the drill bit faces serious challenges. The Polycrystalline Diamond Compact (PDC) bits pull and shear rock by means of PDC cutters, which has the advantage of high rock breaking efficiency in soft to medium hard formations. However, when drilling into complex and hard formations, PDC bit is subjected to serious impact and vibration, and PDC cutters are often worn seriously or even broken, which results in short bit life and low drilling efficiency [1-4].

As the cutting element of PDC bit, the performance of PDC cutter has a decisive influence on the rock breaking effect. Good tools are a prerequisite to the successful execution of a job. For PDC cutter materials, there is large difference in thermal expansion coefficient between cobalt and diamond, which will result in the weakening of D-D bonds between diamond grains, a large residual stress will be generated, and the performance of PDC cutters will be degraded [5, 6]. In view of this, researchers have carried out a lot of researches on residual cobalt decobalt technology, and summarized two methods to remove cobalt from diamond skeleton: strong acid soaking method [7-9] and electrochemical method [10-12]. However, in the process of decobalt treatment, tiny pores are generally generated in the materials, which will weaken the strength of PDC cutter. Therefore, during the synthesis of PDC cutters, some scholars have studied the technology of using noncatalytic binders with better thermal stability to replace cobalt. For example, Qian, J. et al. [13] considered using  $MgCO_3$ , A. S. Osipov et al. [14] considered using  $Li_2CO_3$  and  $CaCO_3$ , E. A. Meysam et al. [15] considered using boron carbide, Mashihadikarimi et al. [16] considered using pure Nb, Huang Zhiqiang et al. [17] considered using nano-cobalt as the binders to replace cobalt, improve the

wear resistance and thermal stability of PDC cutters, but the preparation processes of these methods are complicated, and the requirements for synthesis parameters are more demanding.

Graphene is a perfect honeycomb lattice composed of  $sp^2$  hybridized carbon atoms, which has excellent comprehensive properties of light weight, high hardness and breaking strength, and high thermal conductivity [18]. By adding graphene, it helps to form a lubricating protective film on the diamond grains surface, which can reduce the gap and strengthen the bond binding between diamond grains, and the performance of PDC cutter can be improved. Baker Hughes invented graphene-coated diamond particles, the polycrystalline composite cutter was sintered by adding catalysts or other materials between the diamond particles, but the preparation process was complicated and it was difficult to realize [19]. Jilin University studied a method for preparation of diamond composite cutter containing graphene, by adding graphene and cobalt powder into diamond micro-powder, the gap between diamond grains was filled, and the wear resistance and impact toughness of PDC cutter were improved, but this method still relies on the addition of cobalt as a binder, which cannot avoid the adverse effects of cobalt [20, 21]. However, these research ideas can provide important inspiration for the research of this paper.

Therefore, based on the shortcomings that decobalt technology will weaken the material strength of PDC cutter, and the cobalt replacement preparation technologies require harsh conditions, this paper innovatively applied graphene materials to the preparation of PDC cutter without adding binder cobalt and other catalytic substances; the preparation process is simple and feasible. The extraction and bridging effects of graphene are more conducive to strengthening the D-D bond between diamond grains, thereby improving the comprehensive performance such as impact resistance, wear resistance and heat resistance of PDC cutter. Finally, the research of this paper can provide theoretical support for a new high-performance PDC cutter product.

## 2 PREPARATION PROCESS OF GRAPHENE-ENHANCED PDC CUTTER

The preparation of graphene-enhanced PDC cutter includes six steps: raw material pre-treatment, batching, cemented carbide design, assembly, synthetic sintering, and product post-processing.

### 2.1 Raw Material Pre-Treatment

#### 2.1.1 Diamond Micro-Powder Treatment

Diamond micro-powder is the main raw material for synthesizing polycrystalline diamond layer of PDC cutter. The impurities on its surface have a great influence on the properties of PDC cutter, so it is necessary to purify the diamond micro-powder [22, 23].

In order to ensure that the diamond grains will not be damaged under high pressure, the purchased diamond micro-powder must be in a complete crystal form. High temperature alkali treatment and acid solution treatment were taken to remove the impurity on the surface of the diamond micro-powder.

(1) High temperature alkali solution treatment. The diamond micro-powder was mixed with concentrated NaOH in a beaker, and the beaker was placed in a muffle furnace at 400 °C for 30 min to make the mixture fully react. Then the mixture was cooled to room temperature in the furnace and washed to neutral with deionized water. This operation can remove inorganic mineral impurities in the diamond micro-powder.

(2) Acid solution treatment. The alkali treated diamond micro-powder was placed in a strong acid solution mixed with concentrated nitric acid and concentrated hydrochloric acid. Then the mixture was shocked by ultrasonic shock for 60 min, and was washed with deionized water to neutral. Fig. 1 shows the diamond micro-powder solution after rinsing.

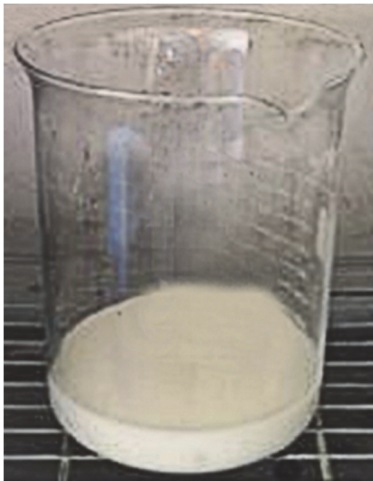


Figure 1 Diamond micro-powder solution after impurity removal treatment

(3) Vacuum drying. The acid treated diamond micro-powder solution was dried in a vacuum oven for 120 min with a pressure of 0,01 MPa and a temperature of 200 °C. The inert gas in the vacuum oven can help to remove various impurities such as water vapor, oxygen, nitrogen and other impurities absorbed on the surface of diamond micro-powder.

#### 2.1.2 Carbide Substrate Treatment

The grade of cemented carbide substrate is YG16, and its cobalt content is 16%. During the synthesis of PDC cutter, cobalt seeps out from the cemented carbide substrate and flows into the diamond micro-powder under high temperature and high pressure, the cobalt acts as a binder to promote the formation of D-D bonds between diamond grains.

Because there are impurities such as oxide scale on the surface of the cemented carbide substrate, which affects the composite strength of PDC cutter, it is necessary to pre-treat the cemented carbide substrate. First, a sand blasting machine was used to blast the surface of cemented carbide substrate to remove impurities, in the meantime fresh surface with tiny pits was exposed so as to increase the contact area between cemented carbide substrate and diamond micro-powder. Then the cemented carbide substrate was cleaned by ultrasonic with acetone and deionized water to remove oil stains and other impurities. Finally, the cemented carbide substrate was dried and placed in a vacuum drying oven for use.

### 2.2 Batching

#### 2.2.1 Diamond Micro-Powder Ratio

According to the classical packing theory, a good particle gradation should be that the void of coarse particles is exactly filled by medium particles, and the void of medium particles is exactly filled by fine particles, thus, the porosity is minimum and the bulk density is maximum [24]. Therefore, the diamond micro-powders with three different particle sizes: coarse particle size (particle size of 30-50 μm), medium particle size (particle size of 5-10 μm) and fine particle size (particle size of 0-1 μm) were selected for proportioning. The particle size mass ratio was  $m_{(30-50\ \mu\text{m})} : m_{(5-10\ \mu\text{m})} : m_{(0-1\ \mu\text{m})} = 70:15:15$ .

#### 2.2.2 Mixing

Due to the large specific surface area, graphene nanosheets have a tendency of spontaneous agglomeration, so the graphene nanosheets need to be uniformly dispersed. Anhydrous ethanol was used as dispersant, and 0,1 wt% graphene nanosheets were added into 100 mL anhydrous ethanol solution, the graphene nanosheets agglomerated and floated above the ethanol, as shown in Fig. 2.

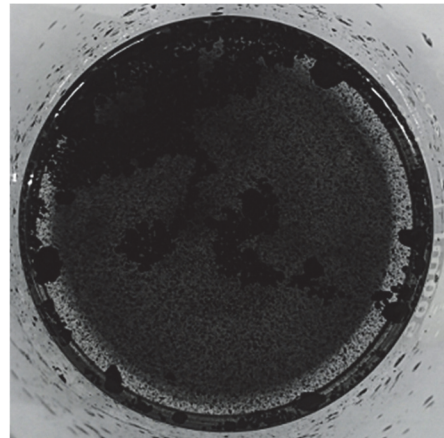


Figure 2 Graphene suspension solution

The above mixed solution was placed in an ultrasonic cleaning device for ultrasonic dispersion for 180 min, the graphene evenly dispersed in the ethanol solution, as shown in Fig. 3.

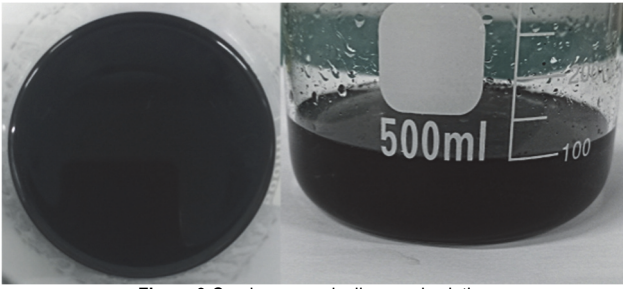


Figure 3 Graphene evenly dispersed solution

The diamond micro-powder with the particle size mass ratio mentioned in section 2.2.1 was fully stirred in the graphene dispersion solution, and ultrasonic dispersion was performed for 60 min. Then, the graphene-diamond dispersion was wet mixed for 200 min in a ball mill mixer. Finally, the wet mixture was placed in a drying oven and dried at 100 °C for 100 min until the mixed powder particles were dispersed and fluffy.

Three kinds of diamond-graphene composite powders with graphene mass percentage of 0,1 wt%, 0,2 wt% and 0,3 wt% were prepared respectively according to the above mixing steps. Meanwhile, pure diamond micro-powder with no graphene added was used as a control group for comparative study.

### 2.3 Carbide Substrate Design

#### 2.3.1 Carbide Substrate Interface Structure Scheme

Due to the great difference in thermal expansion coefficient between the polycrystalline diamond (PCD) layer and the carbide substrate, residual stress is easily generated at the interface between the two, which will lead to the decrease of PDC cutter performance [25, 26]. This is an unavoidable phenomenon, but the problem of residual stress can be alleviated by optimizing the bonding interface structure of cemented carbide substrate.

For the plane shaped bonding interface structure, the contact area between the PCD layer and the carbide

substrate is small, the bonding strength is low, and it is not easy to release the stress, so the bonding interface is usually "grooved" [27]. For the sharp angle, the concentration of residual and impact stresses is easily to be generated, smooth rounded angle is used to replace sharp angle when the interface is grooved. At the same time, the corrugated interface structure helps to disperse the stress and adjust the stress distribution position and direction effectively. Based on this, four kinds of cemented carbide substrate interface structures were designed, and the interface structure was optimized by finite element simulation [28, 29]. Fig. 4 shows the interface structure model of cemented carbide substrates.

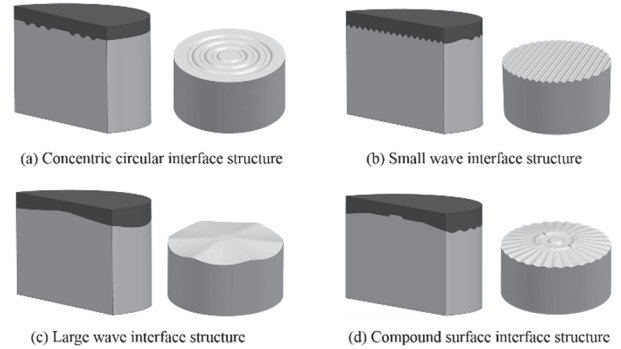


Figure 4 Cemented carbide substrate interface structure

#### 2.3.2 Finite Element Analysis of Thermal Stress of PDC Cutters

The Abaqus thermal-mechanical sequential coupling method was used to optimize the cemented carbide substrate interface structure [30]. The simulation model size ( $\Phi 13,44 \times 8$  mm) was determined according to the actual PDC cutter, and the specific interface structure is shown in Fig. 4. Considering the axisymmetric property of PDC cutter, the 1/2 model was used. It was assumed that there was no plastic deformation occurring in the material during sintering cooling process, and the change of material properties (such as creep) at high temperature was ignored. The physical parameters of PCD layer and carbide substrate (YG16) are shown in Tab. 1.

Table 1 Physical parameters of PCD and carbide substrate

Material	Density / kg/m <sup>3</sup>	Elastic Modulus / GPa	Poisson's ratio	Specific heat (20 °C) / J/(kg·°C)	Thermal Conductivity (20 °C) / W/(m·°C)	Thermal expansion coefficient (20 °C) / $\times 10^{-6} \cdot K^{-1}$
PCD	3510	890	0.22	790	543	2,5
YG16	15000	579	0.07	230	100	5,2

The tetrahedral mesh was used to discretize the model. In order to improve the calculation accuracy, the mesh density was refined, and the mesh size was set to 0,0003 mm. The model mesh division results are shown in Fig. 5.

The upper end face of the PCD layer, the bottom face of the cemented carbide substrate, and the outer peripheral cylindrical surface of both the PCD layer and cemented carbide substrate were fully fixed and restrained. The stress relaxation temperature was set to 1500 °C and the room temperature was 20 °C. The simulation calculation results are shown in Fig. 6 to Fig. 9.

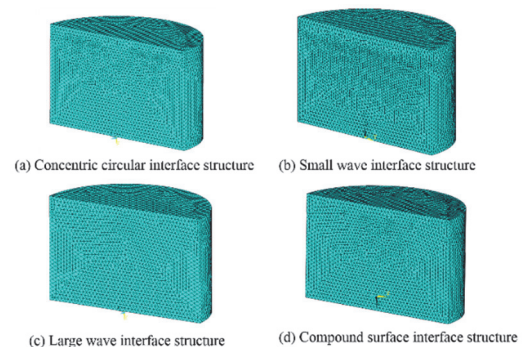


Figure 5 Meshing model

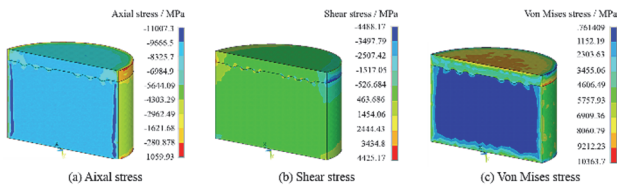


Figure 6 Stress distribution cloud map of concentric circle interface structure

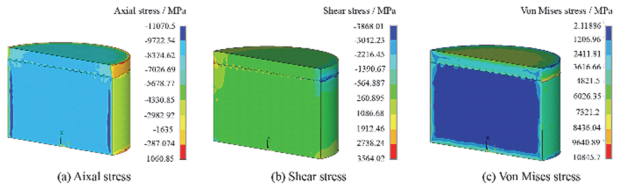


Figure 7 Stress distribution cloud map of small wave interface structure

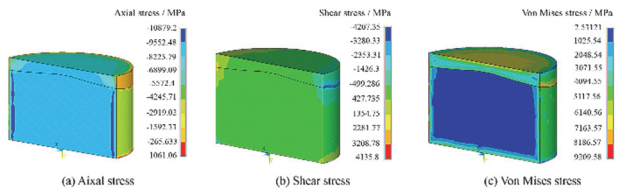


Figure 8 Stress distribution cloud map of large wave interface structure

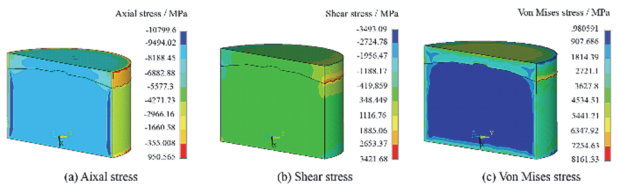


Figure 9 Stress distribution cloud map of compound surface interface structure

In Fig. 6 to Fig. 9, axial stress was analysed according to the principle that tensile stress is positive and compressive stress is negative, and shear stress was analysed according to the principle that clockwise is positive and counter-clockwise is negative.

For all the PDC cutters with four kinds of interface structures, the maximum axial tensile stress was located at the maximum diameter of the upper edge of PCD layer and the lower edge of cemented carbide substrate, the maximum axial compressive stress was located on the cylindrical surface of the cemented carbide substrate near the maximum diameter. The axial compressive stress is beneficial to prolong the life of PDC cutter, while the axial tensile stress can easily lead to the breakage and even delamination of PCD layer. On the basis that the axial compressive stress is required to be as large as possible, it is more important to ensure that the axial tensile stress is as small as possible. The maximum axial compressive stress of PDC cutter with small wave interface structure was the largest, while the maximum axial tensile stress of PDC cutter with compound surface interface structure was the smallest.

Shear stress is the main reason for the delamination of PCD layer and even the fracture of PDC cutter. For all the PDC cutters with four kinds of cemented carbide substrate interface structures, the maximum shear stress was located at the maximum diameter edge of the interface between PCD layer and carbide substrate. The maximum shear stress of PDC cutter with concentric circular interface structure was the largest, while the maximum shear stress

of PDC cutter with compound surface interface structure was the smallest.

The equivalent stress can assist in judging the vulnerable parts of the PDC cutter. For all the PDC cutters with four kinds of cemented carbide substrate interface structures, the maximum equivalent stress was located at the maximum diameter edge of the interface between PCD layer and cemented carbide substrate. The maximum equivalent stress of PDC cutter with small wave interface structure was the largest, while the maximum equivalent stress of PDC cutter with compound surface interface structure was the smallest.

Therefore, considering the axial stress, shear stress and equivalent stress comprehensively, a compound surface interface structure was preferred as the interface shape of the cemented carbide substrate.

### 2.3.3 Validation of Finite Element Method

In order to verify the rationality of the simulation results, taking Xu's paper "Micro-Raman stress of polycrystalline diamond compact" as a reference [31], the simulation results were compared with the Laser Raman test results. The size of the simulation model was consistent with the PDC cutter mentioned in Xu's paper, that is, the diameter of PDC cutter was 25,4 mm, the total thickness was 3,2 mm, and the diamond layer thickness was 0,7 mm. The interface structure of cemented carbide substrate was plane.

Nodes were selected successively along the radial direction on the upper surface of the PCD layer, the simulation and Raman test results of these nodes were compared, as shown in Fig. 10.

According to Fig. 10, the compressive stress showed an overall decreasing trend with the increase of radial distance. The variation rules of the simulation and Raman test results were basically consistent. However, there was a large deviation between the simulation and Raman test results in specific values. The reasons can be summarized as follows: (1) In the simulation, the thermal expansion coefficient of PCD layer was set singly, and its change with temperature was ignored; (2) The stress relaxation temperature also has an effect on the final stress value [32]. There may be a gap between the simulation and the actual situation. (3) The surface of PCD layer will be lapping in the process of PDC cutter, and the lapping will have a certain impact on the surface stress of PCD.

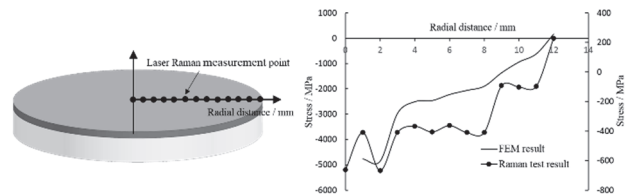


Figure 10 The curve of the stress on the PCD layer with the radial distance

However, although there was a large deviation between the Laser Raman test data and simulation result, the overall variation rule can be referred to. Hence, it was feasible for qualitative comparative analysis of the four kinds of cemented carbide substrate interface structures using this simulation method.

## 2.4 Assembly

The diamond-graphene composite micro-powder and cemented carbide substrate were loaded into a shielding cup. Salt tubes and salt plates in the shielding cup formed a closed space, which can effectively prevent the occurrence of chemical reactions in the phase change layer of leaf paraffin block, and provide a stable high pressure synthesis chamber environment. The components such as salt tube, leaf paraffin block and conductive steel ring were put into a muffle furnace at 120 °C for 8 hours, so as to remove the gas and impurities on the assembled components.

Fig. 11 is the assembly diagram of the synthetic block and the photo of the assembly.

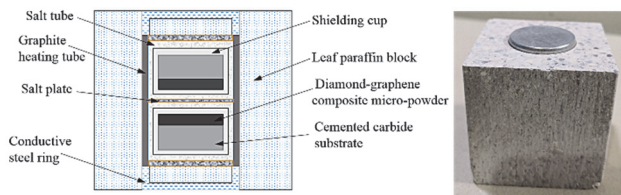


Figure 11 Synthetic block assembly schematic

A total of four kinds of synthetic blocks were assembled: the graphene mass percentage was 0, 0,1 wt%, 0,2 wt% and 0,3 wt% respectively. The corresponding PDC cutters were numbered No. 0, No. 1, No. 2 and No. 3 respectively.

## 2.5 Synthetic Sintering

PDC cutters were synthesized in a cubic synthetic diamond press with a cylinder diameter of 560 mm and a maximum loading pressure of 6 GPa. Photo of the press is shown in Fig. 12. Before synthesis and sintering, the pressure and temperature of the press were calibrated by fixed point standard pressure method and thermocouple method to ensure the accuracy of synthetic parameters [33].

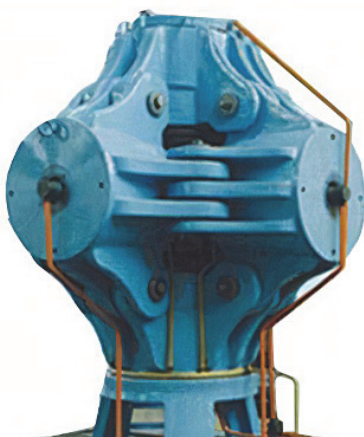


Figure 12 Photo of cubic synthetic diamond press

Synthesis temperature, pressure and time are three key parameters affecting the sintering performance of PDC cutter. In general, the higher the synthetic pressure, the better the density and wear resistance of the PDC cutter, but the higher the requirements for the press. The synthesis temperature and synthesis time are not the higher the better

or the lower the better. It is necessary to comprehensively consider the wear resistance of PDC cutter, micro cracks and other defects of diamond layer and overburning problems [34].

The synthesis was carried out by means of increasing the pressure first then sending the temperature, cooling the temperature first then releasing the pressure. The internal cavity of the synthesis block was 5,5-6 GPa, the synthesis temperature was 1500 °C, and the synthesis time was 750 s. The synthesis process curve is shown in Fig. 13.

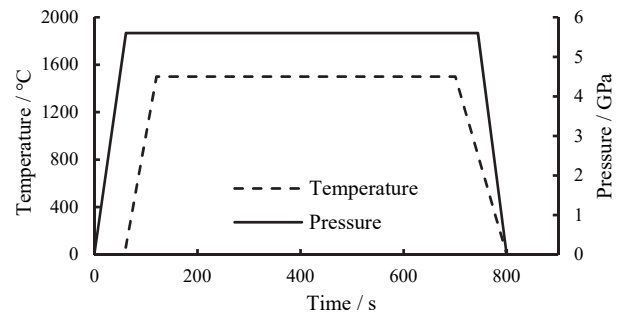


Figure 13 Synthesis process curve

No. 0, No. 1, No. 2 and No. 3 PDC cutters were sintered normally, and no defects were found on the surface of PCD layers. Fig. 14 shows the PDC cutters after sintering and synthesis.

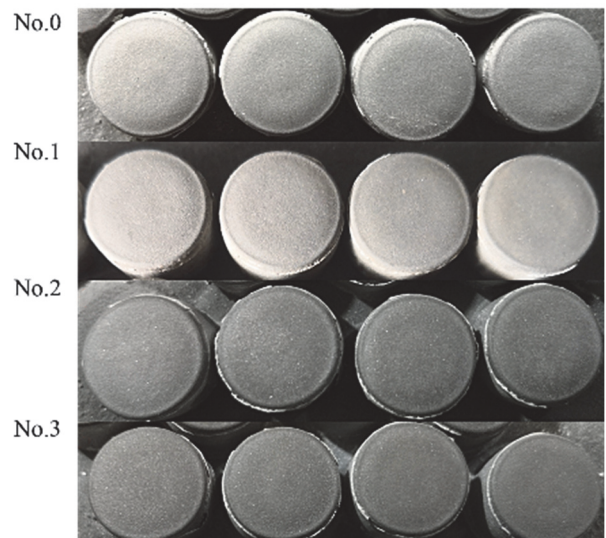


Figure 14 Photos of four groups of PDC cutters

## 2.6 Post-Processing

The synthesized PDC cutters were machined to the standard size. The PDC cutters were roughly ground and finely ground by cylindrical grinder and centerless grinder respectively, the impurities on the surface of the cutters were removed, and the outer diameter of the cutters was ground to the standard outer diameter of 13,44 mm. Surface grinding machine was used to grind the bottom surface of the cutters' cemented carbide substrate to a standard height of 8,0 mm.

Fig. 15 shows the No. 0, No. 1, No. 2 and No. 3 PDC cutters after machining. Naked eye observation showed that there was no difference in the appearance of the four groups of cutters.

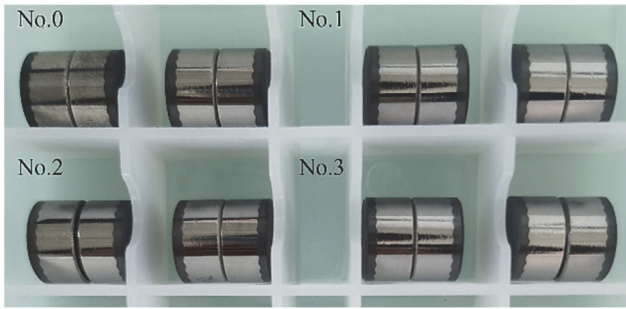


Figure 15 Photos of the four groups of PDC cutters

### 3 PERFORMANCE CHARACTERIZATION OF GRAPHENE-ENHANCED PDC CUTTER

The properties of the above four groups of PDC cutters were characterized from two aspects: microscopic morphology and macroscopic mechanical properties.

#### 3.1 Microscopic Morphology

Phenom desktop scanning electron microscope was used to observe and analyse the bonds between diamond particles and the distribution of binders. First, SEM samples of PDC cutters were prepared by wire-electrode cutting, and the cutting surfaces were polished until they became a mirror. Fig. 16 shows the SEM samples of PDC cutters.



Figure 16 Samples of PDC cutters for SEM

Fig. 17 shows the SEM microstructures of the four groups of scanned PDC cutters.

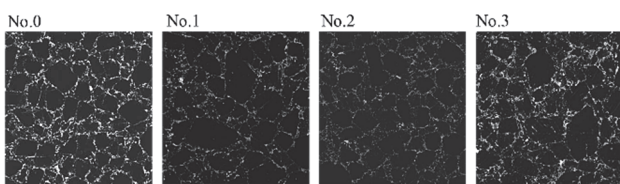


Figure 17 SEM microstructure images of four groups of PDC cutters

As shown in Fig. 17, for No.0 PDC cutter without graphene added, the white binder distributed around the black diamond grains in a network structure, and the binders showed spot-like aggregation in individual areas. The binder wrapped around the diamond grains affected the bonding (D-D bonds) between diamond grains. For No. 1 PDC cutter with 0,1 wt% graphene added and No. 2 PDC cutter with 0,2 wt% graphene added, the brightness of the white binder decreased significantly, and the binder was flocculent along the diamond grain boundary. The lubrication characteristics of graphene contribute to the sharp reduction of friction between diamond grains, and the bonding between diamond grains was dense. However, when the amount of graphene addition was increased to 0,3 wt% (No. 3 PDC cutter), the white binder showed flake

distribution, and the diamond grains were separated by the binder. There may be a problem of graphene agglomeration, which hindered the bonding between diamond grains and caused uneven dispersion of the binder.

Fig. 18 is a SEM microstructure diagram of the interface between cemented carbide substrate and diamond layer. For the four groups of PDC cutters, the cemented carbide and diamond grains were interlaced with each other at the interface, the bonding was firm, and no metal agglomeration occurred [35].

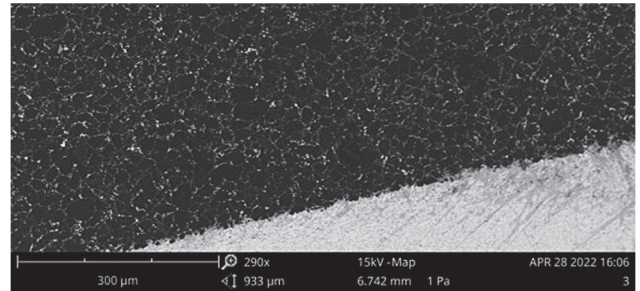


Figure 18 SEM micrograph of the interface between cemented carbide substrate and diamond layer

#### 3.2 Macroscopic Mechanical Properties

##### 3.2.1 Heat Resistance Test

After the muffle furnace was heated to 800 °C, the four groups of PDC cutters were placed in the muffle furnace for naked burning. When the furnace was heated to the specified temperature, the samples were removed and placed in white corundum to cool to room temperature. Fig. 19 shows the test process.

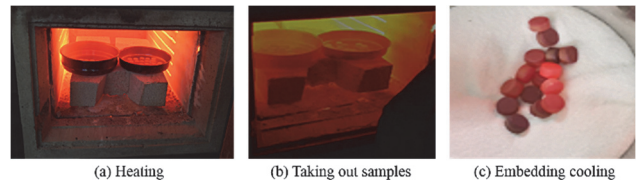


Figure 19 Heat resistance test process

After heating, the defects of PCD layer of the four groups of PDC cutters were observed, as shown in Tab. 2.

According to Tab. 2, when the temperature rose to 880 °C, there were no cracks on the PCD surface of the four groups of PDC cutters. When the temperature rose to 890 °C, network cracks appeared on the PCD surface of the two No. 0 PDC cutters and the two No. 2 PDC cutters, tortoise cracks appeared on the PCD surface of the one No. 1 PDC cutter, and no cracks appeared on the PCD surface of the two No. 2 PDC cutters.

The reasons can be summarized as follows:

(1) There was no graphene added for No. 0 PDC cutter, the network shaped binder expanded at 890 °C, and the expansion force exceeded the bounding force between diamond grains, so network cracks occurred in all No. 0 PDC cutters.

(2) At room temperature, the thermal expansion coefficients of graphene and cobalt binder are  $8,0 \times 10^{-6}/K$  and  $12 \times 10^{-6}/K$  respectively. The internal expansion force of the PDC cutter with graphene added is less than that of the PDC cutter without graphene added. Therefore, the heat

resistance of No. 1 and No. 2 PDC cutters was better than that of No. 0 PDC cutter.

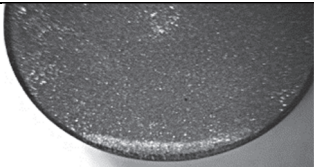
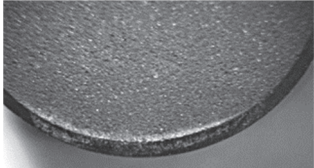
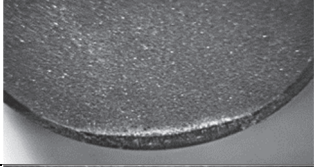
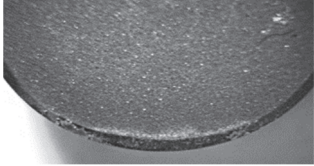
(3) There was a large amount of graphene in No. 3 PDC cutter, and SEM results showed that the internal binder was unevenly dispersed. During heat resistance test, a large stress source was easily formed in the binder agglomeration area, thus causing surface cracks on PCD surface.

In addition, at room temperature, the thermal conductivity of graphene and diamond is 5000 W/(m·K) and 2000 W/(m·K) respectively, so the overall thermal conductivity of PDC cutter with graphene added is also improved. Friction heat generated on the cutters during drilling can be diffused more quickly, which helps to extend the life of PDC cutters.

Table 2 Heat resistance test results of PDC cutters

PDC cutter	Temperature	
	880 °C	890 °C
No. 0		
No. 1		
No. 2		
No. 3		

Table 3 Wear resistance test data of PDC cutters

PDC cutter	Average mass wear of the grinding wheel / g	Average grinding time / s	Average mass wear ratio / $\times 10^4$	Wear morphology of PDC cutter
No. 0	119,355	127,6	18	
No. 1	119,14	160,5	28	
No. 2	124,825	132,5	41	
No. 3	124,85	288,5	32	

### 3.2.2 Abrasion Resistance Test

PDC cutters are fixed on the PDC bit body by brazing at a temperature of about 700~800 °C. In order to be close to the actual working conditions, the PDC cutters were heated to 750 °C and kept for 15 min, then the wear resistance tests were carried out.

The wear resistance of PDC cutter was evaluated by mass wear ratio according to "JB/T 3235-2013 determination method of wear ratio of polycrystalline diamond" [36]. The grinding wheel size used in the test was 100 × 16 × 20 mm. The grinding time was set based on grinding a grinding wheel with the same diameter. The mass wear ratio is expressed as:

$$E_m = (M_s / M_j) \times \eta \tag{1}$$

where:  $E_m$  is the mass wear ratio;  $M_s$  is the mass wear of the grinding wheel, g;  $M_j$  is the mass wear for PDC cutter, g;  $\eta$  is the correction factor for grinding wheel, generally takes 1,02.

Two pieces of cutters from each group of PDC cutter were taken for testing. The mass wear ratio of each group of PDC cutter was obtained by averaging the mass wear ratio of the two pieces of cutters. The results and grinding morphology of the PCD layer are shown in Tab. 3.

According to Tab.3, the mass wear ratio of PDC cutters with graphene added was higher than that of PDC cutter without graphene added. The mass wear ratios of No. 2 and No. 3 PDC cutters were both  $30 \times 10^4$  higher, and they were high wear ratio PDC cutters. The grinding wheel speed of No. 0 and No. 2 PDC cutters was obviously faster than that of No. 1 and No. 3 PDC cutters, so the grinding wheel capacity of No. 0 and No. 2 PDC cutters was stronger. After grinding, the cutting edges of the four groups of PDC cutters were all worn normally, and the cutting edge of No. 3 PDC cutter bore the least wear, which was considered to be related to its weak ability to grind the grinding wheel. The wear ratio of No. 2 PDC cutter was 127,8% higher than that of No. 0 PDC cutter without graphene added.

### 3.2.3 Impact Resistance Test

Similar to the wear resistance test, the PDC cutters were first heated to 750 °C and kept for 15 min before the impact resistance test was carried out. A drop hammer impact test was used. PDC cutters were fixed on the punch head with a fixed elevation angle of 20°. The punch pin continuously impacted the mold steel with a given energy. The hardness of the mold steel was HRC58-62. For each punch impact, the mold steel rotated 10° to ensure that the PDC cutter can impact the undamaged mold steel plane each time. Fig. 20 shows the drop hammer impact test device.

The impact energy was loaded in a step-by-step style. Starting from a single impact energy of 30 J, after every 10 impacts, the single impact energy was successively increased by 10 J, until the final single impact energy reached 70 J. During the impact process, when the PCD layer was damaged, the test was stopped, and the total impact energy that PDC cutter can withstand was

calculated according to the cumulative energy of a single impact.

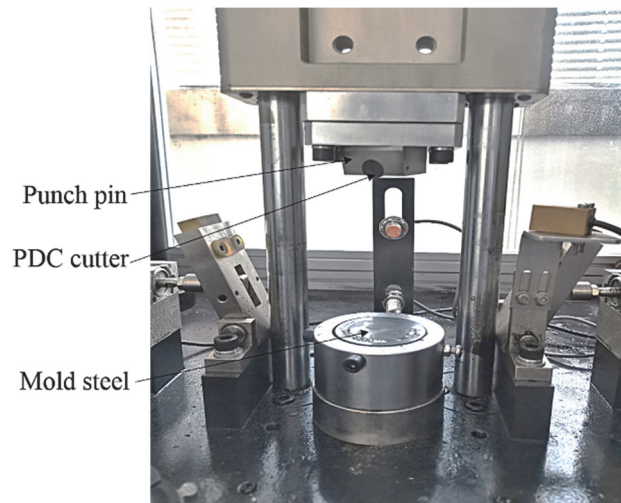


Figure 20 Drop hammer impact test device

Two pieces of cutters from each group of PDC cutters were taken for testing. The impact energy of each group of PDC cutter was obtained by averaging the impact energy of the two pieces of cutters. The results and damage morphology of the PCD layer are shown in Tab. 4.

According to Tab. 4, the impact times of the four groups of PDC cutters were all at a high level (more than 40 times). For No. 2 and No. 3 PDC cutters, the impact times were full marked 50, and the impact energy was 2500 J, cracks were formed at the interface between PCD layer and cemented carbide substrate in both No. 2 and No. 3 PDC cutters. For No. 0 and No. 1 PDC cutters, the impact energy was similar, and the PCD layer fragmentation occurred in both of them.

Table 4 Impact test data of PDC cutters

PDC cutter	Average number of impacts	Cumulative average impact energy / J	Sample damage morphology
No. 0	43	2010	
No. 1	45	2150	
No. 2	50	2500	
No. 3	50	2500	



### 3.4 Comprehensive Characterization of Cutter Performance

The Multiple Attribute Decision Making method [37, 38] was used to comprehensively select the optimal PDC cutter scheme from the aspects of microscopic morphology, heat resistance, wear resistance and impact resistance.

There are  $A_i (i = 1, 2, \dots, m)$  alternatives, which are  $A_1$  (No. 0 PDC cutter),  $A_2$  (No. 1 PDC cutter),  $A_3$  (No. 2 PDC cutter) and  $A_4$  (No. 3 PDC cutter) respectively. There are  $X_j (j = 1, 2, \dots, n)$  attributes, which are  $X_1$  (microscopic morphology),  $X_2$  (heat resistance),  $X_3$  (wear resistance) and  $X_4$  (impact resistance) respectively. The attribute values of each scheme are shown in Tab. 5.

**Table 5** Attribute value of each PDC cutter scheme

Scheme	Attribute			
	$X_1$	$X_2$	$X_3$	$X_4$
$A_1$	Good binder distribution	880 °C	$18 \times 10^4$	2010
$A_2$	Excellent binder distribution	880 °C	$28 \times 10^4$	2150
$A_3$	Excellent binder distribution	890 °C	$41 \times 10^4$	2500
$A_4$	Medium binder distribution	880 °C	$32 \times 10^4$	2500

The representations in  $X_1$  are quantified, with scores of 9, 7, and 5 for good, excellent and medium respectively. Therefore, the decision matrix can be expressed as:

$$D = d_{ij} = \begin{bmatrix} d_{11} & d_{12} & d_{13} & d_{14} \\ d_{21} & d_{22} & d_{23} & d_{24} \\ d_{31} & d_{32} & d_{33} & d_{34} \\ d_{41} & d_{42} & d_{43} & d_{44} \end{bmatrix} = \begin{bmatrix} 7 & 880 & 18 \times 10^4 & 2010 \\ 9 & 880 & 28 \times 10^4 & 2150 \\ 9 & 890 & 41 \times 10^4 & 2500 \\ 5 & 880 & 32 \times 10^4 & 2500 \end{bmatrix} \quad (2)$$

According to the equation:

$$r_{ij} = d_{ij} / \sum_{i=1}^m d_{ij} \quad (3)$$

The decision matrix is normalized:

$$R = r_{ij} = \begin{bmatrix} r_{11} & r_{12} & r_{13} & r_{14} \\ r_{21} & r_{22} & r_{23} & r_{24} \\ r_{31} & r_{32} & r_{33} & r_{34} \\ r_{41} & r_{42} & r_{43} & r_{44} \end{bmatrix} = \begin{bmatrix} 0,233 & 0,249 & 0,151 & 0,219 \\ 0,3 & 0,249 & 0,235 & 0,235 \\ 0,3 & 0,253 & 0,345 & 0,273 \\ 0,167 & 0,249 & 0,269 & 0,273 \end{bmatrix} \quad (4)$$

The information entropy method is used to calculate the weight of each attribute. The entropy of  $A_i$  to attribute  $X_j$  is:

$$E_j = -k \sum_{i=1}^m (r_{ij} \ln r_{ij}) = -\frac{1}{\ln m} \sum_{i=1}^m (r_{ij} \ln r_{ij}) \quad (5)$$

Combining Eqs. (4) and (5), it can get:

$$E = [E_1 \ E_2 \ E_3 \ E_4] = [0,98153 \ 0,99998 \ 0,97104 \ 0,99674] \quad (6)$$

The discrimination degree of  $X_j$  to scheme  $A_i$  is:

$$F_j = 1 - E_j \quad (7)$$

The attribute weight of each scheme is:

$$w_j = F_j / \sum_{j=1}^n F_j \quad (8)$$

According to Eqs. (6) and (7), the attribute weight value is:

$$w = w_j = [w_1 \ w_2 \ w_3 \ w_4]^T = [0,364228 \ 0,000394 \ 0,571091 \ 0,064287] \quad (9)$$

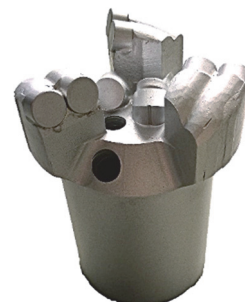
The final solution decision is obtained from the decision matrix and attribute weight. The simple weighted sum method is used, the comprehensive value of scheme  $A_i$  for all attributes is:

$$v_i = \sum_{j=1}^n v_{ij} = \sum_{j=1}^n r_{ij} w_j \quad (10)$$

According to Eq. (4), Eq. (9) and Eq. (10), the final decision values of  $A_1, A_2, A_3$  and  $A_4$  are 0,1853, 0,2587, 0,3239 and 0,2321 respectively. Scheme  $A_3$  (No. 2 PDC cutter) shows the highest decision value, so its comprehensive performance is the best.

## 4 REAL DRILLING TEST

Real drilling tests were carried out for No. 0, No. 1, No. 2 and No. 3 PDC cutters to further evaluate the comprehensive performance of PDC cutters, also to verify the performance characterization results obtained in Section 3. The above four groups of PDC cutters were brazed to  $\Phi 94$  mm three wing concave bit body (shown as Fig. 21), and the real drilling tests were carried out.



**Figure 21**  $\Phi 94$  mm three wing concave PDC bit


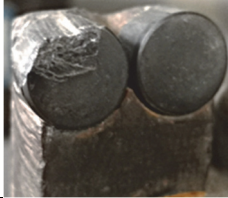


The test site was Baiping Coal Mine of Zhengmei Group, the construction borehole was the bottom gas drainage hole, and the drilling rock was mainly limestone, with coal-containing interlayer, and the rock Platts hardness was about 7. The drilling rig used in the drilling field was the ZDY3200 drilling rig produced by Xi'an Research Institute of China Coal Science and Industry Group, the drill pipe was  $\Phi 63,5$  mm auger pipe. The drilling test results are shown in Tab. 6.

According to Tab. 6, the concave bit welded No.2 PDC cutters showed the largest footage in both rock and coal, and its average rate of penetration reached 15,4 m/h, which was significantly higher than that of the PDC bit welded

other cutter samples. The concave bit welded No. 3 PDC cutters drilled in the whole rock section, and its average rate of penetration was 10.5 m/h, which was the lowest.

Observing the wear of the PDC cutters of each PDC bit, the wear of No. 0 and No. 1 PDC cutters was the most serious, and there was large volume of wear, also the peeling of diamond layer occurred in No. 1 PDC cutters. The wear of No. 2 PDC cutters was the least. Considering the drilling parameters and the wear state of the PDC cutters, the real drilling performance of No. 2 PDC cutter was the best, this result also is consistent with that obtained in Section 3.

**Table 6** Real drilling test results

PDC cutter	Bit footage		Average rate of penetration / $\text{m}\cdot\text{h}^{-1}$	Cutter wear condition
	Footage in rock / m	Footage in coal / m		
No. 0	17,52	8,76	12,3	
No. 1	14,6	4,38	12,8	
No. 2	18,25	12,41	15,4	
No. 3	18,25	0	10,5	

## 5 CONCLUSION

Based on the excellent mechanical and thermal properties of graphene, this paper innovatively applied graphene materials to the preparation of PDC cutter, no binder cobalt addition was required, which can avoid the decobalt process. Also the preparation process was simple and feasible. The performance evaluations of PDC cutters with different graphene added were carried out from two aspects of microscopic morphology and macroscopic mechanical properties, and the Multiple Attribute Decision Making method was used to evaluate the optimal graphene added scheme. The PDC cutter with 0,2 wt% graphene added showed the best comprehensive performance, comparing with the commonly used PDC cutter without graphene added, its heat resistance increased by 10 °C, wear ratio increased by 127,8%, and the impact energy increased by 24,4%. Real test results showed that the concave drill bit with 0,2 wt% graphene added PDC cutters

showed the fastest average ROP, the least cutter wear, and the best drilling effect. The research of this paper breaks through conventional products, greatly improves the comprehensive performance of PDC cutter, and provides theoretical guidance for the market application of the new graphene-enhanced PDC cutter product. In the future, we will focus on the field drilling test of 0,2 wt% graphene added PDC cutter, to fully verify its performance, and provide a large amount of data support for its market application.

## Acknowledgements

This research was supported by Natural Science Basic Research Project of Shaanxi Province, grant number 2021JQ-952, and Science and Technology Innovation Fund Project of CCTEG Xi'an Research Institute, grant number 2021XAYJCQ02. We appreciate their support very much.

## 6 REFERENCES

- [1] Wang, C. (2021). Feasibility study on the principle of punching-shearing composite rock fragmentation mode of connecting holes in rock strata. *Coal Geology & Exploration*, 49(3), 244-248. <https://doi.org/10.3969/j.issn.1001-1986.2021.03.031>
- [2] Ju, P., Tian, D., Wang, C., & Tian, H. (2021). Theoretical and simulation analysis on rock breaking mechanical properties of arc-shaped PDC bit. *Energy Reports*, 7, 6690-6699. <https://doi.org/10.1016/j.egy.2021.09.148>
- [3] Ju, P. (2019). Cutter load distribution analysis and crown shape optimal design of complex curved PDC bit. *Journal of Engineering and Technological Sciences*, 51(1), 14-27. <https://doi.org/10.5614/j.eng.technol.sci.2019.51.1.2>
- [4] Zhang X., Meng, Q., Yu, M., Zhang, Z., & Guo, Z. (2021). Coal Rock Breaking Simulation and Cutting Performance Analysis of Disc Cutters. *Technical Gazette*, 28(5), 1755-1761. <https://doi.org/10.17559/TV-20210423115559>
- [5] Moseley, S., Bohn, K., & Goedickemeier, M. (2009). Core drilling in reinforced concrete using polycrystalline diamond (PCD) cutters: Wear and Fracture Mechanisms. *International Journal of Refractory Metals & Hard Materials*, 27(2), 394-402. <https://doi.org/10.1016/j.ijrmhm.2008.11.014>
- [6] Fan, P., Xu, Q., Yi, C., Dong, P., & Lan, H. (2017). Effect of cobalt removal on thermal stability of polycrystalline diamond. *Journal of Material Science & Engineering*, 35(1), 87-90. <https://doi.org/10.14136/j.cnki.issn1673-2812.2017.01.017>
- [7] Wang, C., Liu, H., & Fang, H. (2019). A study on cobalt removal technique and wear resistance of polycrystalline diamond compact at indoor temperature. *Superhard Material Engineering*, 31(2), 30-34. <https://doi.org/10.3969/j.issn.1673-1433.2019.02.010>
- [8] Gou, R., Luo, X., Li, K., Kang, C., & Chen, J. (2022). PCD after cobalt leaching reinforced by high temperature annealing: Tribo-logical properties and graphitization evolution. *Diamond and Related Materials*, 125, 108988. <https://doi.org/10.1016/j.diamond.2022.108988>
- [9] Yi, X. & Zhang, S. (2020). A method for strengthening polycrystalline diamond compact cutter. Chinese patent: 202010665551.5, 2020-03-22.
- [10] Guo, Z., Deng, F., Zhang, L., Zhang, Zi., Wang, H., Zheng, K., Gao, Y., & Fang, Y. (2022). The novel and facile electrolysis method for removing the cobalt binder phase from large diameter polycrystalline diamond compacts. *Ceramics International*, 48(3), 3125-3132. <https://doi.org/10.1016/j.ceramint.2021.10.086>
- [11] Liu, C., Kou, Z., He, D., Chen, Y., Wang, K., Hui, B., Zhang, R., & Wang, Y. (2012). Effect of removing internal residual metallic phases on wear resistance of polycrystalline diamond compacts. *International Journal of Refractory Metals and Hard Materials*, 31, 187-191. <https://doi.org/10.1016/j.ijrmhm.2011.10.014>
- [12] Zhang, Y., Yang, K., Liu, R., Zheng, M., Li, P., Liu, G., Zhang, Y., Liu, J., Li, M., Fu, Q., & Yang, Q. (2019). Electrolyte for re-moving cobalt, method for surface modification of diamond compact cutter. Chinese patent: 201710784412.2, 2019-08-27.
- [13] Qian, J., McMurray, C., & Mukhopadhyay, D. (2013). Polycrystalline diamond cutters sintered with magnesium carbonate in cubic anvil press. *International Journal of Refractory Metals and Hard Materials*, 31, 71-75. <https://doi.org/10.1016/j.ijrmhm.2011.09.008>
- [14] Osipov, A., Klimczyk, P., & Cygan, S. (2017). Diamond-CaCO<sub>3</sub> and diamond-Li<sub>2</sub>CO<sub>3</sub> materials sintered using the HPHT method. *Journal of the European Ceramic Society*, 37, 2553-2558. <https://doi.org/10.1016/j.jeurceramsoc.2017.02.028>
- [15] Ekimov, E., Ralchenko, V., & Popovich, A. (2014). Synthesis of superconducting boron-doped diamond compacts with high elastic moduli and thermal stability. *Diamond & Related Materials*, 50, 15-19. <https://doi.org/10.1016/j.diamond.2014.09.001>
- [16] Mashhadikarimi, M. (2017). Obtaining triple layer polycrystalline diamond compact by HPHT method. Universidade Federal do Rio Grande do Norte.
- [17] Huang, Z., Yan, Y., Li, Q., & Yuan, Y. (2018). Effect of nano Co addition on properties of PDC composite plate. *Heat Treatment of Metals*, 43(10), 14-19. <https://doi.org/10.13251/j.issn.0254-6051.2018.10.004>
- [18] Liu, Y. (2017). *Graphene: From basics to applications*. Beijing: Chemical Industry Press.
- [19] Chakrabeti, S., Digiovanni, A., Agrawal, G., Scott, D., & Mathur, V. (2016). Diamond particles coated with grapheme, including the composition and spatial structure of such particles, and a method for forming diamond particles and polycrystalline composite cutter coated with graphene. Chinese patent: 201180058106.1, 2016-04-13.
- [20] Chen, Z., Ma, D., Wang, S., Dai, W., Li, S., Zhu, Y., & Liu, B. (2020). Effects of graphene addition on mechanical properties of polycrystalline diamond compact. *Ceramics International*, 42(8), 11255-11260. <https://doi.org/10.1016/j.ceramint.2020.01.150>
- [21] Xiao, G., Zhang, C., Zou, B., & Zou, G. (2021). A polycrystalline diamond compact cutter with graphene and its preparation method. Chinese patent: 201910659163.3, 2021-07-13.
- [22] Zhang, Y., Zhang, J., Lv, R., Fang, L., Li, Y., Qin, J., & Kou, Z. (2018). Discussion on the sintering problem of fine grain PCD. *Diamond and Abrasive Engineering*, (6), 61-64. <https://doi.org/10.13394/j.cnki.jgsz.2008.06.013>
- [23] Liu, B. (2005). *Research on functionally graded polycrystalline diamond-cemented tungsten carbide composite button insert*. Jilin: Jilin University.
- [24] Liu, H. (1991). Particle size distribution and packing theories. *Journal of Silicates*, 19(2), 164-172.
- [25] Kanyanta, V. & Ozbayraktar, S. (2014). Maweja, K. Effect of manufacturing parameters on polycrystalline diamond compact cut-ting tool stress-state. *International Journal of Refractory Metals and Hard Materials*, 45, 147-152. <https://doi.org/10.1016/j.ijrmhm.2014.03.009>
- [26] Mukhopadhyay, D. (2021). Identifying the causes of residual stress in polycrystalline diamond compact (PDC) cutters by X-Ray diffraction technique. *Results in Materials*, 11, 100216. <https://doi.org/10.1016/j.rinma.2021.100216>
- [27] Xu, G., Chen, F., Xu, G., & Xiao, J. (2007). Residual stresses analysis of polycrystalline diamond compacts with different interface. *Superhard Material Engineering*, 19(4), 10-14. <https://doi.org/10.3969/j.issn.1673-1433.2007.04.002>
- [28] Zhang, Z. (2016). Ways of decreasing the residual stress in polycrystalline diamond compacts. *Superhard Material Engineering*, 28(5), 49-53. <https://doi.org/10.3969/j.issn.1673-1433.2016.05.010>
- [29] Chen, F., Xu, G., Ma, C., & Xu, G. (2010). Thermal residual stress of polycrystalline diamond compacts. *Transactions of Nonferrous Metals Society of China*, 20(2), 227-232. [https://doi.org/10.1016/S1003-6326\(09\)60126-6](https://doi.org/10.1016/S1003-6326(09)60126-6)
- [30] Liu, Y., Su, S., Huang, H., & Liang, Y. (2019). Thermal-mechanical coupling buckling analysis of porous functionally graded sandwich beams based on physical neutral plane. *Composites Part B: Engineering*, 168, 236-242. <https://doi.org/10.1016/j.compositesb.2018.12.063>
- [31] Xu, G., Yin, Z., Chen, Q., & Xu, G. (2010). Micro-Raman stress of polycrystalline diamond compact. *Journal of Central South University (Science and Technology)*, 41(4), 1310-1314.
- [32] Bertagnolli K. & Vale R. (2000). Understanding and controlling residual stresses in thick polycrystalline diamond

- cutters for enhanced durability. *Proceedings an International Technical Conference on Diamond, Cubic Boron Nitride and their Applications, Vancouver*.
- [33] Zhang, C. (2020). *Study on the effect of synthesis pressure on the polycrystalline diamond compact*. Jilin: Jilin University.
- [34] Sun, Y. (2011). *Research on synthesis and mechanism of boron-doped polycrystalline diamond (PDC) compact*. Beijing: General Iron and Steel Research Institute.
- [35] Ahmadian, M., Wexler, D., Chanadra, T., & Calka, A. (2005). Abrasive wear of WC-FeAl-B and WC-Ni<sub>3</sub>Al-B composites. *International Journal of Refractory Metals and Hard Materials*, 23(3), 155-159.  
<https://doi.org/10.1016/j.ijrmhm.2004.12.002>
- [36] *National Technical Committee for Standardization of Abrasive and Abrasive Tools*. Beijing: China Machine Press, 2014.
- [37] Tuğba, D., Evrencan, Ö., & Tamer, E. (2022). Personnel selection with multi-criteria decision making methods in the ready-to-wear sector. *Technical Gazette*, 29(4), 1339-1347.  
<https://doi.org/10.17559/TV-20210816220137>
- [38] Julio, C., Gonzalo, N., & Yamisleydi, S. (2022). Normalization method for quantitative and qualitative attributes in multiple attribute decision-making problems. *Expert Systems with Applications*, 198, 116821.  
<https://doi.org/10.1016/j.eswa.2022.116821>

**Contact information:**

**Pei JU**, Associate Researcher

(Corresponding author)

Xi'an Research Institute of China Coal Technology & Engineering Group Corp,  
82. jinye 1st Road, Xi'an National Hi-tech Industrial Development Zone,

Xi'an 710077, China

E-mail: jpnt2005@163.com

**Chuanliu WANG**, Associate Researcher

(Corresponding author)

Xi'an Research Institute of China Coal Technology & Engineering Group Corp,  
82. jinye 1st Road, Xi'an National Hi-tech Industrial Development Zone,

Xi'an 710077, China

E-mail: wangchuanliu@cctegxian.com